

## A compound sensor for biomechanical analyses of buttock soft tissue *in vivo*

Jue Wang, MS; David M. Brienza, PhD; Ying-wei Yuan, PhD; Patricia Karg, MS; Qiang Xue, PhD  
*University of Pittsburgh, Department of Rehabilitation Science and Technology, Forbes Tower, Room 5052, Pittsburgh, PA 15260; Advanced Devices Company, 52 Dragon Court, Suite 1B, Woburn, MA 01801*

**Abstract**—A sensor for *in vivo* biomechanical characterization of buttock soft tissue has been developed and evaluated. The sensor measures interface pressure, applied force, tilt, and rotation angle of the sensor head, and the thicknesses of multiple soft tissue layers. A composite ultrasonic transducer using a 1-3 ceramic-polymer structure was developed for the sensor. The sensor can identify subcutaneous soft tissue interfaces 5 to 65 mm below the skin surface with a 0.26-mm axial resolution, pressure over the range of 0 to 68 kPa, and force over the range of 0 to 3.6 kg. Our purpose for developing the sensor was to study the biomechanical characteristics of buttock soft tissues. Successful identification of distinguishing characteristics in persons with a susceptibility to pressure ulcers may result in the development of a risk assessment tool based on tissue characterization.

**Key words:** *compound sensor, interface pressure, normal force, pressure ulcer prevention, tissue deformation, ultrasound.*

This material is based upon work supported in part by the Paralyzed Veterans of America, Spinal Cord Research Foundation, Washington, DC 20006-3517; The Rehabilitation Engineering Research Center on Wheeled Mobility, The School of Health and Rehabilitation Sciences, University of Pittsburgh, Pittsburgh, PA 15260.

Address all correspondence and requests for reprints to: Jue Wang, MS, University of Pittsburgh, Department of Rehabilitation Science and Technology, Forbes Tower, Room 5052, Pittsburgh, PA 15260; email: [juewang@pitt.edu](mailto:juewang@pitt.edu).

### INTRODUCTION

Prevention of pressure ulcers is an important health care issue. In 1994, there were an estimated 1.5 to 3 million individuals in the United States with pressure ulcers (1). In hospitals, estimates of the incidence of pressure ulcers vary from 2.7 to 29.5 percent (1–4). However, estimates of the incidence of pressure ulcers increase to 60 percent in tetraplegic populations and to 66 percent in elderly patient populations with hip fracture (2,4). An estimated 50 to 80 percent of people with spinal cord injuries (SCI) develop pressure ulcers (5). The risk of death increases fourfold with the development of a pressure ulcer among geriatric patients and inhabitants of nursing homes (2,6–8). The annual cost of treating pressure ulcers in hospital settings is estimated to be as high as \$6.4 billion (4).

Over the past 30 years, research has increased our understanding of the factors leading to the formation of pressure ulcers. Pressure ulcers usually occur over bony prominences (9). Pressure-induced occlusion of capillary blood flow, resulting in tissue ischemia, is considered to be the primary cause (10,11). Interface pressure measurement, among other factors, is used clinically to evaluate

and prescribe support surfaces for clients at risk of developing pressure ulcers. However, the accuracy, limitations, and implications of pressure measurements have been questioned (12–15). Several investigators have suggested deformation of tissue as an important indicator. Graebe advocated the use of “deformation patterns” to establish an individual’s tolerance to external loading (16). Levine et al. (12) proposed that tissue shape and deformation measurements are superior to interface pressure measurements in characterizing the loading condition between the buttocks and a seat support surface. Reddy pointed out that an adequate model should consider the responses of tissue matrix (deformation), and the responses of blood and lymphatic and interstitial fluid (17).

Despite these expert opinions advocating the use of deformation measurement, there are no practical clinical methods available for direct measurement of buttock tissue deformation for a person in a seated posture. In 1986, Reger et al. used MRI techniques to study human buttocks tissue in response to external support loading (18). They measured soft tissue thickness changes from skin to ischium for spinal cord-injured and able-bodied subjects in the supine position. However, due to constraints of the imaging device, the subject could not be evaluated while sitting. Therefore, the method could not be used to study biomechanical properties of buttock tissue with subjects in a normal seated posture. In 1996, Brienza et al. used a Computer Automated Seating System (CASS) to measure tissue stiffness as an indicator of soft tissue deformation, to optimize support surface shape (19). They investigated cushion contour optimizations for 30 elderly subjects (age 65 years or older) and 12 SCI patients (20). Integration of ultrasonic transducers into the CASS was proposed as a way to extend the device’s capabilities to include direct measure of tissue response to loading (21).

Ultrasound pulse-echo techniques frequently have been used to study the morphological and pathological state of tissues in a controlled environment. Sehgal et al. (22) investigated ultrasound transmission and reflection computerized tomography for imaging bones and adjoining soft tissue. Krouskop et al. (23) used gated ultrasonic doppler to determine variations in elastic modulus of tissue properties and to measure residual limb shape for CAD prosthetic sockets. Kadaba et al. (24) investigated the feasibility of using ultrasound to detect incipient pressure ulcers. He proposed that velocity and backscatter might be useful in differentiating normal and pressure-damaged muscle tissue. Clark et al. (25) used B-mode ultrasound to measure the thickness of soft tissue over the sacrum of

elderly patients to identify those patients likely to develop pressure ulcers. In 1991, a method for quantitative measurement of strain and elastic-modulus distribution in soft tissues using ultrasound and the cross-correlation analysis technique was described by Ophir et al. (26). In 1996, Zheng and Mak (27) built an ultrasonic indentation system that used a hand-held indentation probe and assessed the response of the soft tissue covering the volar side of the first metacarpal of a human subject.

This manuscript describes the development and evaluation of a compound sensor for use in the previously developed CASS (19,28; **Figure 1**). The most recent version of the CASS comprises an 11 by 12 array (43×47 cm) of support elements for which the height is computer controlled to vary loading conditions and surface shape. A pressure transducer is fixed in the center of a swiveling head on top of a group of 96 support elements located front

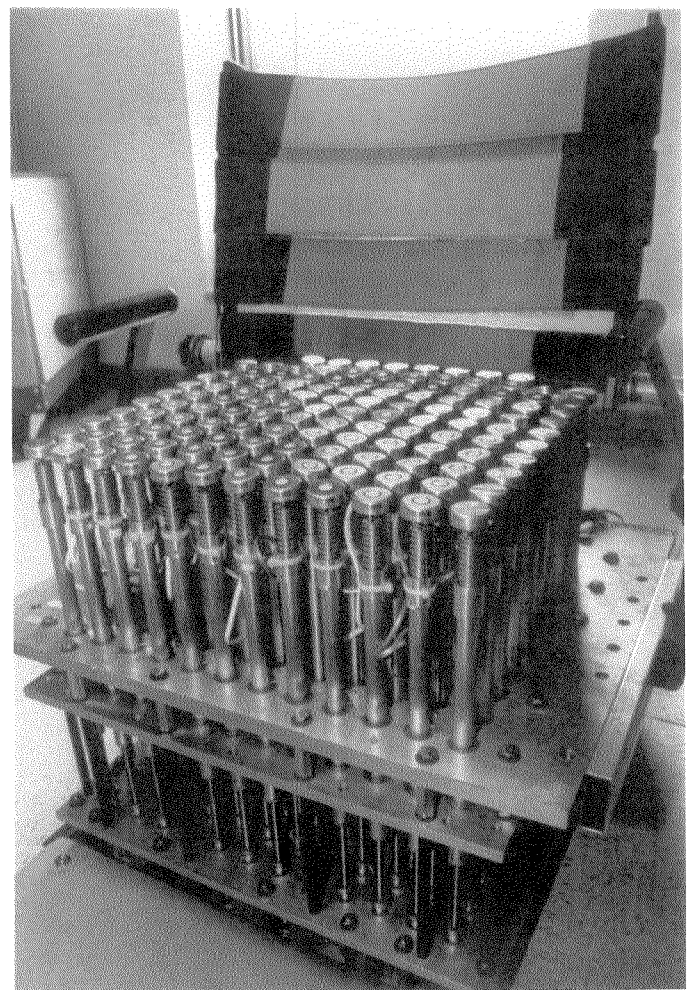


**Figure 1.**  
The Computer Automated Seating System (CASS).

and center on the seating surface. The compound transducers measure pressure, force, tissue layer thickness, and orientation of the CASS sensor head. A novel, composite ultrasonic transducer using a 1-3 ceramic-polymer structure was designed and developed for this sensor. Our goal was the simultaneous measurement of tissue layer thickness, interface pressure, applied force, and sensor head orientation during an indentation test of the buttock tissue to study their interrelationships in dynamic loading and unloading. The development of the sensor is intended to enhance the capability of the CASS to allow the characterization of buttock soft tissue *in vivo*. Future studies using this capability may lead to findings concerning the tissues' susceptibility to pressure ulcer formation.

## DESIGN AND DEVELOPMENT

### Structure of the Compound Sensor

The structure of the compound sensor is shown in **Figure 2**. On the swiveling head, a pressure transducer is fixed in the center and four ultrasonic transducers are evenly distributed around the pressure transducer. The swiveling head can freely tilt and rotate by means of a ball joint so that the pressure and ultrasonic transducers are oriented in a direction normal to the direction of net force. The tilt angle of the swiveling head is detected by a linear potentiometer attached on the side surface of the sensor body. The rotation angle is detected by a circular, wire-wound potentiometer located on top of the sliding cylinder. A force sensor adapted from a recent version of the seating system (29), composed of four bonded-foil strain gauges mounted on an aluminum cantilever beam, is located in the bottom of the sensor body. The vertical force applied to the sensor is transmitted to the cantilever beam by a steel piston with a conical point at the end that comes in contact with the beam. A stepper motor (Superior Electric Co., Bristol, CT) is connected to the sensor body by an ACME lead screw and an actuator tube, allowing adjustment of the vertical position of the sensor through a range of approximately 15 cm. Nine compound sensors form a 3 by 3 subset array (12×12 cm) on the CASS surface in the area of one ischial tuberosity (IT) on the pelvis.

### Potential Modes of Operation

The measurements from the compound sensors in the enhanced CASS may be used in three operating modes. In operating mode 1, a single ultrasound channel is selected

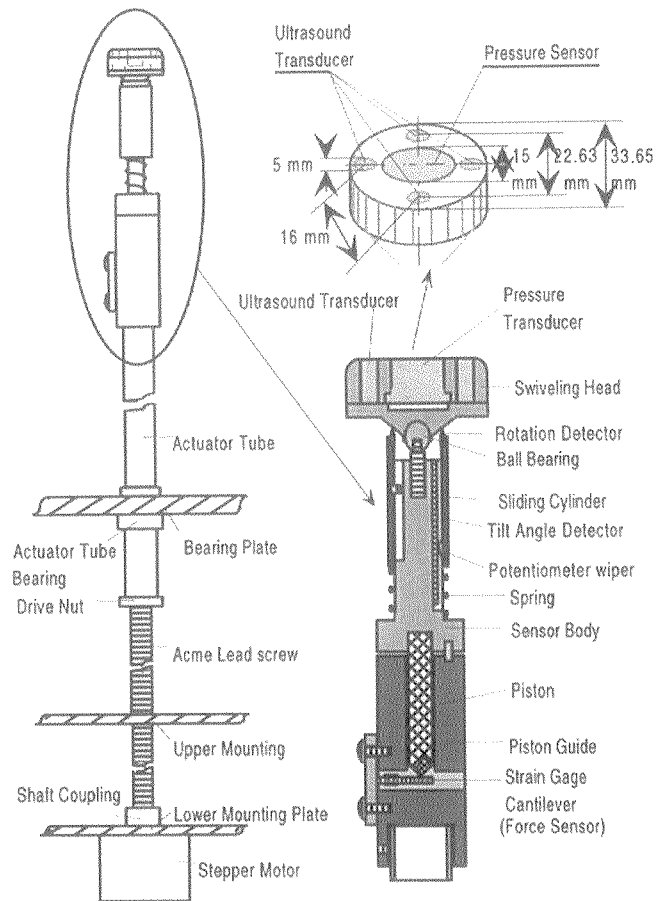


**Figure 2.**  
The structure of a compound sensor.

for use in a load-indentation test. The channel and sensor are selected based on their location relative to the area of interest on the buttocks and the quality of the ultrasound echo signal as observed in an initial scan of all channels. The thicknesses of fat, muscle, and bulk tissue layers, interface pressure, force, and tilt angle are simultaneously measured as the sensor moves through indentation, hold, and recovery cycles. Data recorded during the cycle are used to approximate response of load-bearing soft tissue above the selected sensor. The pilot experiments presented in this paper were performed using operating mode 1.

Because the ultrasound transducers are offset from the center of the sensor's swiveling head, the soft tissue measurements do not coincide with the pressure and force measurements located at the center of the head. To compensate for this offset, operating mode 2 combines the measurements from the four ultrasonic transducers evenly distributed around the center of the head. (The sensor head is shown in **Figure 2**.) The mean distance from each of the four perimeter transducers to the target interface is a good

first-order approximation of the distance from the center of the sensor head to the target interface.

As an alternative to the two operating modes described above, the 36 ultrasonic transducers in the compound sensor subset array may be combined to generate 3-D point cloud-like images of the soft tissue and bony structures of the area around one IT. This 3-D shape information could be combined with information from previously generated solid models of the pelvis to determine the approximate position and orientation of the pelvis while a person is seated on the CASS.

### Determination of Ultrasonic Transducer Parameters

The development of a small, long-cabled ultrasonic transducer with high sensitivity, high resolution, and a high signal-to-noise ratio (S/N) was the key to producing the compound sensor. The established design of the CASS constrained the geometry of the ultrasonic transducer. The overall size of the swiveling head is 33.65 mm in diameter by 11.6 mm high. To integrate the ultrasonic transducer into the CASS design, it needed to have a diameter <5 mm, height <7.2 mm, and a 3-m cable for connecting from the seating surface to a 36-channel ultrasound data acquisition and interface system. Hence, each ultrasonic crystal was limited in diameter to only 3 mm. On the other hand, to meet the requirements of soft tissue analysis, an emitting frequency of 7.5 MHz was chosen to achieve the desired 5 to 65 mm measurement range. Our application required that the loop sensitivity of the transducer exceed  $-22$  dB at an output electrical impedance of  $50 \Omega$ . Tradeoffs between small size and high sensitivity and among the high emitting frequency, long cable, and low noise were necessary.

Axial resolution is an important parameter of an ultrasonic transducer. It is affected by bandwidth, damping (ring down) characteristics, and ultrasound field characteristics. To investigate the deformation of subcutaneous soft tissue layers and to identify the properties of these tissues, ring down of  $0.8 \mu\text{s}$  at  $-20$  dB and  $1.2 \mu\text{s}$  at  $-40$  dB damped from the peak magnitude was required. For a transducer excited by a sinusoidal signal, with a diameter of 3 mm and using a 7.5 MHz single frequency, an undulatory pressure contour in a near-field zone of 11.25 mm is expected. The development of damping and ultrasound field characteristics required the transducer to have a broad fraction bandwidth.

### Ultrasonic Transducer Design

A novel composite ultrasonic transducer using a 1-3 ceramic-polymer structure with double coupling layers

was selected for use in the compound sensor. Due to its special structure and the use of a soft polymer material with lower acoustic impedance, the composite ultrasonic transducer has several advantages over conventional transducers (30,31). First, it has a higher thickness-coupling coefficient (kt), ranging from 60 to 75 percent. Second, it has less spurious oscillating modes, improving the S/N of the measurement. Third, the 1-3 ceramic-polymer composite has low acoustic impedance to better match the soft tissue, thus allowing ultrasound energy to penetrate into soft tissue more easily. The composite transducer not only improves the sensitivity of the measuring system, but also expands the frequency bandwidth, enhancing the axial resolution of the detection. In addition, the composite transducer has been designed to have precise electrical impedance to match with electronic circuitry so that transmission line loss is minimized and emitting/receiving efficiency is maximized.

## RESULTS AND EVALUATION

### Ultrasonic Transducer Performance

An acoustic intensity measurement system, AIMS-01 (NTR Systems, Inc., Seattle, WA 98107), was used to measure acoustic field characteristics of the transducer: it consisted of a BA-2020 RF buffer amplifier, a DG-2200 delay/gate generator, a WD-4000 wave form digitizer, and a digital oscilloscope (100 MHz). An ultrasound measurement system developed at the University of Pittsburgh was used to evaluate the axial resolution of the transducer. An HP 4193A vector impedance meter (0.4–110 MHz, Hewlett-Packard Co., Palo Alto, CA 94304) was used to measure electric impedance of the transducer. The measurement of the sound field was performed in the standard water tank of the AIMS-01 system. An analysis of the ultrasound field is presented in the Appendix.

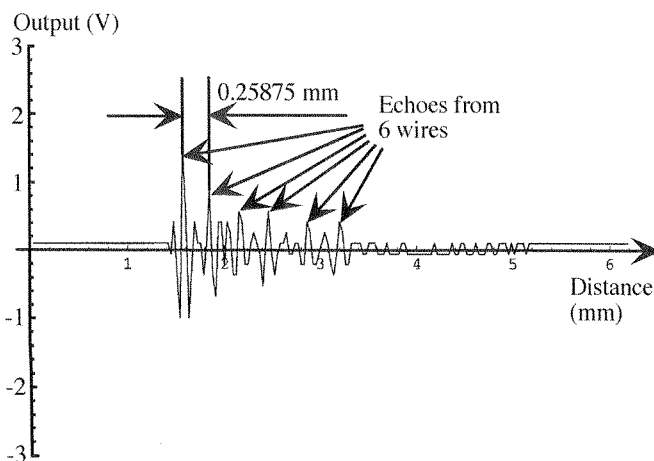
Two conventional ceramic, lead zirconate titanate (PZT) transducers and a 1-3 piezo-composite ceramic transducer were assessed and compared. The results are summarized in **Table 1**. The composite ultrasonic transducer showed many desirable characteristics. The sensitivity of a composite ultrasonic transducer is 9–13 dB higher than an homogeneous PZT ceramic transducer. The bandwidth is wider by 39–47.7 percent and its pulse width is reduced by more than  $0.065 \mu\text{s}$ . The axial resolution was improved to 0.26 mm. In addition, although the cable of the composite transducer is 3 meters long, it can achieve a S/N of 45 dB.

**Table 1.**

Comparison of properties between composite and conventional ultrasound transducers.

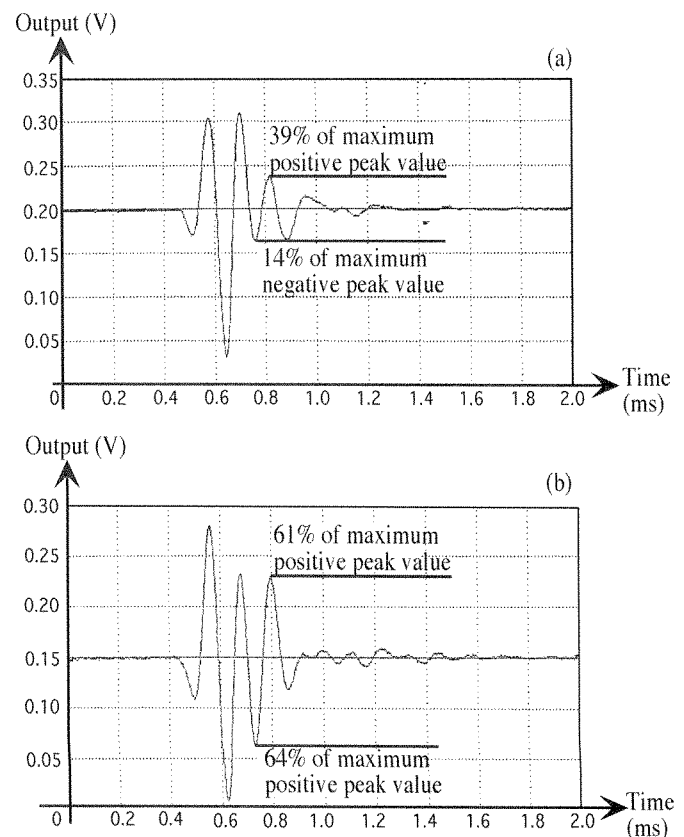
Parameter	Composite	Conventional PZT 1	Conventional PZT 2
Sensitivity	-22 dB	-31 dB	-35 dB
Bandwidth (-3 dB)	81.71%	42.72%	34.01%
Bandwidth (-6 dB)	98.7%	53.3%	43.9%
Center Frequency	7.506 MHz	7.157 MHz	8.136 MHz
Pulse Width	0.165 $\mu$ s	0.23 $\mu$ s	0.295 $\mu$ s
Axial Resolution	0.26 mm	0.6 mm	0.6 mm
Cable Length	3 m	2 m	2 m

The loop sensitivity was calculated in decibels as the ratio of peak-to-peak echo voltage to pulse voltage (into 50  $\Omega$ ). Pulse width was calculated from the integral of the pulse intensity as 1.5 times the rise time (the time required to go from 10 percent to 90 percent of its final value). **Table 1** also shows the bandwidths when the ultrasound energy attenuates -3 dB and -6 dB of the maximum magnitude of the spectrum. Axial resolution of the transducer was obtained by using 6 copper wire targets with a diameter of 0.12 mm placed into a water tank. As the transducer detected the 6 targets, we gradually increased the distances between the wires until the signal on the monitor of the measurement system could clearly distinguish these 6 targets. The result from a composite transducer is shown in **Figure 3**. The axial resolution was determined to be 0.26 mm.

**Figure 3.**

An ultrasound echo trace showing the axial resolution of an ultrasound transducer. The echoes from six wire targets show axial resolution of at least 0.26 mm.

The damping characteristics of the transducers were evaluated by time-domain analysis of the echo waveform properties. The transducers received echoes from a distance of 12 mm. The echo waveforms of the composite transducer and the conventional PZT transducer are compared in **Figure 4 (a)** and **(b)**. For the composite transducer with -22 dB gain, the third positive voltage peak is 39 percent of the maximum positive peak voltage, and the third negative voltage peak is 14 percent of the maximum negative peak voltage. For the conventional PZT transducer with -35 dB gain, the third positive voltage peak is 61 percent of the maximum positive peak voltage, and the third negative voltage peak is 64 percent of the maximum negative peak voltage. The beam profile of the composite transducer was measured by scanning its sound field. The receiver was a hydrophone placed 40.5 mm from the center of the ultrasonic transducer's surface. The scanning size was 75  $\times$  12 mm and an incremental step of 1 mm was used during the scan. **Figure 5** shows

**Figure 4.**

Comparison of the characteristics in time area between a composite ultrasonic transducer and a conventional PZT ultrasonic transducer (a) Composite transducer (Gain: -22 dB, 9-foot cable length); (b) PZT transducer (Gain: -35 dB, 6-foot cable length).

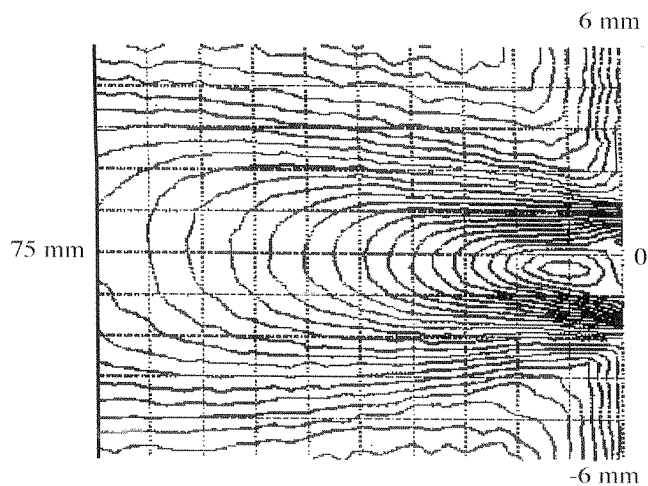


**Figure 5.**  
The sound-field characteristics of the composite transducer shown as a 2-D contour map.

a 2-D planar scan-contour plot of an ultrasound field of a composite transducer with a beam waist near 0.4 mm in diameter. Each contour represents a 1-dB decrease of magnitude in sound pressure from the center. At the point where the magnitude of the ultrasound field drops 3 dB, the beam width is 1.0 mm in diameter at the maximum intensity position and is 5.4 mm in diameter at a detecting distance of 54.5 mm from the transducer.

## Properties of the Compound Sensor

### 1. Compatibility of the Ultrasound Coupling Material

The compound sensor simultaneously measures both interface pressure and ultrasound echoes from its surface. Therefore, the influence of the ultrasound coupling material on interface pressure measurements was investigated. The pressure calibration device and method

used were described by Brienza et al. (19). When using ultrasound gel as the coupling material, the standard deviation of the pressure data was  $3.45 \times 10^{-2}$  kPa. When using nylon as the coupling material, the standard deviation of the pressure data was 0.55 kPa. The ultrasound gel produced the most reproducible results, with a relative error less than 6 percent.

### 2. Specifications of the Compound Sensor

The calibration of the sensor was carried out using the CASS. A 36-channel ultrasound system was developed and integrated into the CASS. A GageScope 50-MHz high-speed data acquisition card (Gage Applied Science, Inc., South Burlington, VT) was used for digitizing the ultrasound signal with 8-bit resolution. The DAP 1204E Data Acquisition processor (Microstar Laboratories, Inc., Bellevue, WA) with 12-bit resolution was used to measure pressure, force, and tilt angle data. Two CIO-DIO-96 digital I/O boards (CyberResearch, Inc., New Haven, CT) were used for selecting the ultrasound pulse and receiver channels, and for controlling the motor array. An 8-axis step motor controller (UCN-5804B model, Allegro MicroSystems, Inc., Worcester, MA) was used for controlling the position of the motor array. An 80486 PC was used for controlling the array of motors and a 200-MHz PC was used for high level control of the system. The computers communicate using the serial port for controlling the CASS motors and for synchronous sampling. The software for motor control was developed using Turbo Pascal 7.0, and other components are implemented in LabVIEW 5.0.

The properties of the compound sensor are summarized in **Table 2**. The compound sensor can identify subcutaneous soft tissue interfaces 5 mm to 65 mm below the

**Table 2.**  
The specifications of the Compound Sensor.

Param	Ultra	Press	Force	Tilt	Rotat	Motor
Range	5-65 mm	0-68 kPa	0-3.6 kg	-45°-+45°	16°-360°	14.8 cm
Sens	-22 dB	0.17 kPa	24 g	0.4°	--	--
Res	0.26 mm	0.17 kPa	24 g	0.4°	1.5°	1 mm
S/N	45 dB	--	--	--	--	--
N/L	<1.2%	<0.5%	<0.25%	--	--	--
S/R	--	--	--	--	--	≤1,500
L/D	--	--	--	--	--	0-45 N
RMS	--	≤0.36	≤0.24	≤0.96	--	--
Rel	--	≤8%	≤5%	≤4%	≤2.8%	≤3%

Param=parameter, Ultra=ultrasound transducer; Press=pressure transducer; Force=force sensor; Tilt=tilt angle, Rotat=rotation angle; Sens=sensitivity; Res=resolution; S/N=signal-to-noise ratio; N/L=non-linearity; S/R=step rate in steps per s; L/D=load/drive capability; RMS=root mean square error; REL=relative error.

skin surface (Figure 6) with good linearity ( $R^2$  is 0.999934 in static water target test) over the entire range, a 0.26-mm axial resolution,  $-22$  dB sensitivity, and 45 dB S/N. The sensor can measure pressure from 0 to 68 kPa with less than 0.5 percent non-linearity, and provides 0 to 3.6 kg force detection with less than 0.25 percent non-linearity, 24 g resolution and less than 5 percent measurement error. The sensor can also measure  $\pm 45^\circ$  of tilt angle with  $0.4^\circ$  resolution, as well as measure up to a  $244^\circ$  rotation angle with  $1.5^\circ$  resolution. The motor system has load-driving capability of up to 45 N, a height control range of 14.8 cm with 1 mm resolution, and can be driven at speeds up to 1,500 steps per second with less than 3 percent relative error.

### Pilot Experiment

A preliminary *in vivo* test was performed using the enhanced CASS. A male subject (Body Mass Index:  $20.5 \text{ kg/m}^2$ ) was seated on the CASS support surface with his right IT positioned on the 3 by 3 compound sensor array subset. An indentation test was performed with indentation, hold, and recovery phases of the cycle. The speed of

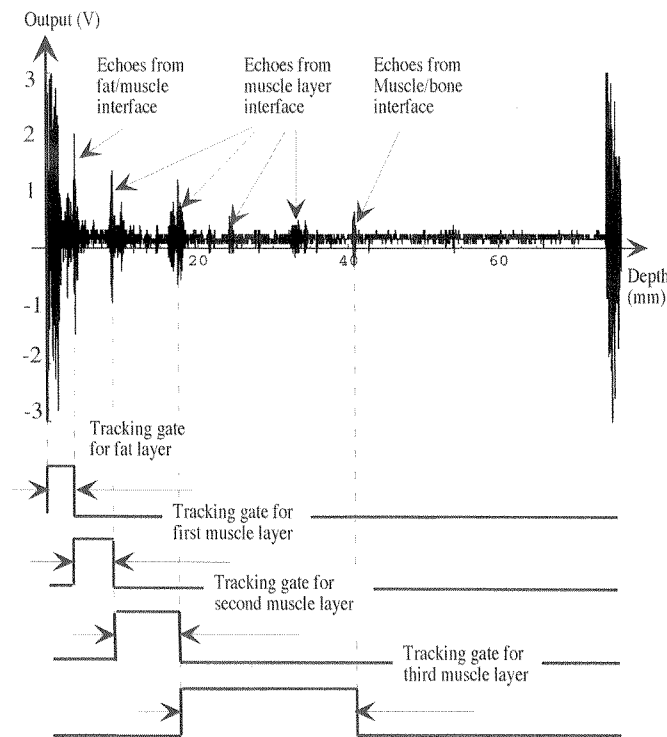


**Figure 6.**

An ultrasound echo trace from a human thigh. The peaks of the traces correspond to various subcutaneous soft tissue interfaces at the distances indicated.

loading and unloading was 0.53 mm/sec, the total indentation was 10 mm, and the sensor probe was held for 26.4 s at maximum indentation. The thicknesses of multiple tissue layers were acquired by timing the width of ultrasonic echo tracking gates (see Figure 6). Data, including pressure, force, sensor head tilt angle, and thicknesses of multiple tissue layers, were simultaneously recorded for three trials over the same anatomic site. The interval time between trials was less than 20 s. The results are shown in Figure 7. The parameters have a corresponding time-phase relationship. Typical normal force-deformation characteristics for the three trials are shown in Figure 8. Figure 9 displays the linear relationship between interface pressure and normal force ( $R^2=0.99$ ).

### DISCUSSION AND CONCLUSIONS

The initial testing of the compound sensor has successfully demonstrated its ability to assess buttock soft tissue under controlled loading conditions. An *in vivo* test was performed in which interface pressure, force, tilt angle, and tissue thicknesses in fat and bulk tissue layers were simultaneously recorded under dynamic loading conditions. Figure 7 shows a typical data set. Traces for pressure, force, tilt angle, and thicknesses of fat, and bulk

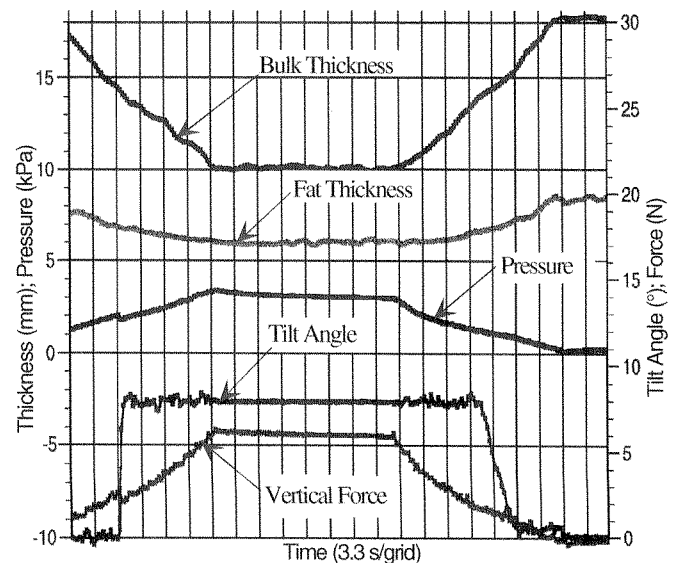


**Figure 7.**

Data collected during an *in vivo* load indentation test on a human subject for soft tissue near the right ischial tuberosity. The correspondence between bulk tissue thickness, fat layer thickness, external pressure, tilt angle, and vertical force is shown.

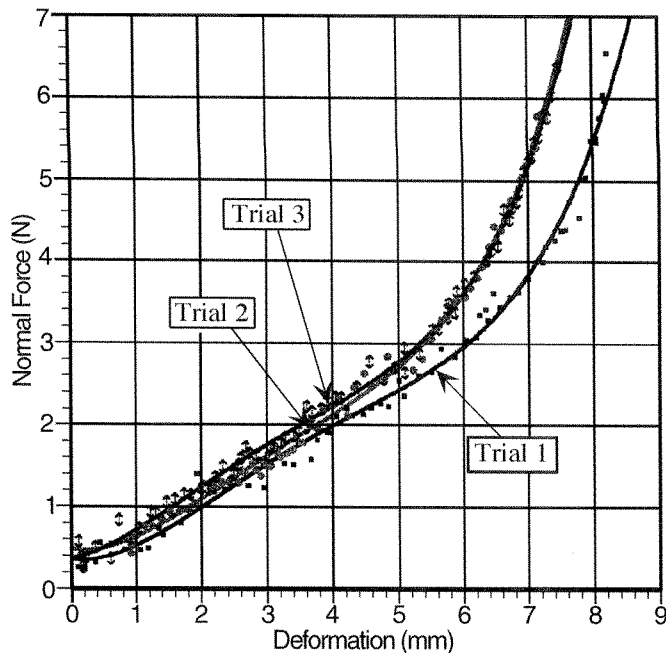


**Figure 8.**  
Force-deformation characteristic in recovery phase for three trials.

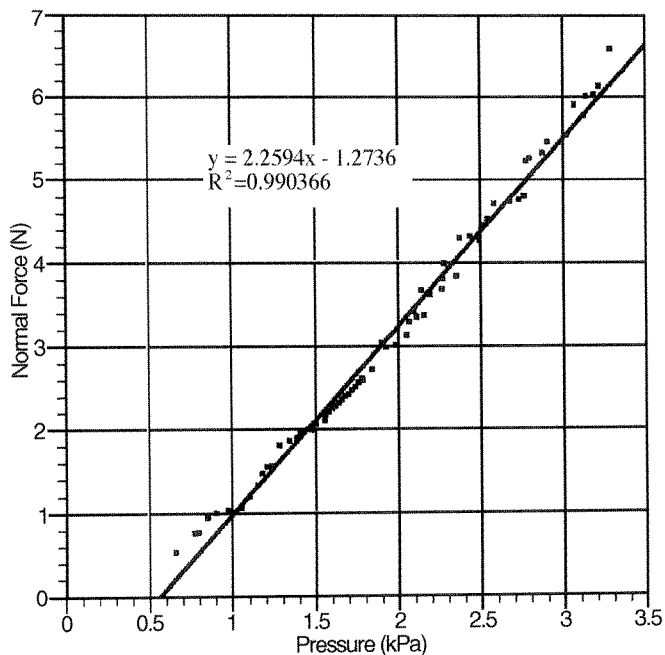


**Figure 9.**  
Relationship between interface pressure and normal force.

tissue are shown. This and other similar tests demonstrate the ability of the system to collect the desired data.

Analysis of the results of our initial experiments was used to make several preliminary observations regarding the characteristics of our measurement system. The relationship between normal force and tissue deformation was extracted from the recovery phase in three trials (**Figure 8**). The data from trial 2 and trial 3 show the consistency of the measurement. The differences between trial 1, and trials 2 and 3 indicate that the viscous response of *in vivo* soft tissues is reduced after repeating loading and unloading. The maximum slopes in the force-deformation curves increase with successive loading/unloading cycles. This behavior illustrates the need for preconditioning when assessing viscoelastic properties of soft tissue. The relationship between interface pressure and normal force was linear (**Figure 9**), suggesting that the swiveling head of the sensor reduces shear force in the loaded tissues under test conditions. Overall, the pilot results demonstrate that the compound sensor has the ability to investigate and to quantify the complex relationships among the biomechanical parameters of buttock soft tissue during loading.

This successful development of the compound sensor provides the foundation for future development of various signal-processing techniques to enhance our systems' measurement capabilities. Three operating modes were described in this paper. In mode 1, a time-domain signal-processing technique, ultrasonic cross-correlation, can be used for a more quantitative assessment of loading stress and soft tissue strain to estimate tissue elasticity. This is important for assessing tissue integrity. In mode 2, an interpolation technique using four ultrasonic transducers located on a single sensor can be used to compensate for error in measurement related to the spatial correspondence between the ultrasonic and other measurements. The tissue thickness measurements from the four ultrasonic transducers can be used to predict the deformation of tissues located over the center of loading.

Both mode 1 and mode 2 are limited to measure only the axial component of the total tissue deformation. In mode 3, ultrasonic transducers in a 6 by 6 planar array can be used together to generate a 3-D visualization of soft tissue interfaces. This capability may allow the estimation of lateral components of soft tissue deformation. The position and orientation of the pelvis can also be determined if its shape has been determined beforehand.

Our pilot testing has confirmed several limitations in using ultrasound to analyze buttock soft tissue properties. The IT is conical in shape and the projected area is comparable in size to the sensor's area. The irregular shape of the pelvis affects the acquisition of ultrasound echoes

because the bone interface is not always perpendicular to the ultrasound beam during dynamic loading. This results in the loss of echo tracking during dynamic loading conditions. In addition, although the swiveling head of the sensor can freely tilt and rotate in compliance with buttock tissue, decreasing interface friction and shear forces, it increases the measurement error and affects the acquisition of echoes from deep tissue such as muscle and bone interface.

Another limitation of the system is related to the characteristics of ultrasound propagation through tissues with different densities. In the CASS system, the weight-bearing pelvis presses down onto the buttocks and onto the associated tissues, such as the gluteus maximus muscle, deep fascia, fat, subcutaneous tissue, dermis, and epidermis. Ultrasound propagates at different velocities in different soft tissue layers. The estimates of tissue thickness assume a uniform tissue density, therefore introducing measurement error when this assumption does not hold true.

Our long-term goal is to develop a clinical assessment system to discriminate between tissue at higher or lower risk of pressure ulcer development. The development of the CASS instrumentation is necessary so that we can compare differences in intrinsic soft tissue mechanical characteristics. Comparisons between populations we know to be at high risk, such as persons with SCI who have histories of pressure ulcer development and subjects without any known risk factors, may lead to the discovery of distinguishing characteristics. Our enhanced instrumentation has the potential to lead to significant findings concerning the biomechanics of buttock soft tissue and its susceptibility to pressure ulcers. For example, a tissue deformation measurement combined with the measurement of normal force allows for the biomechanical modeling of soft tissue. If model parameters allow for the differentiation between people with a demonstrated lower or higher risk of developing pressure ulcers, a clinical test and/or clinical practice guidelines could be developed to predict and thus prevent pressure ulcers. Such a diagnostic test would be particularly useful in determining pressure ulcer risk.

## APPENDIX

### Analysis of the Ultrasound Field

An analysis of the ultrasound field was performed for the compound sensor. In the CASS system, the ultra-

sonic transducers work sequentially; thus, only one transducer is active at any moment. Therefore, it is assumed that there is no interference between the ultrasound fields generated by adjacent transducers. Thus, the analysis of the entire acoustic field of the compound sensor can be simplified to the analysis of the field for a single transducer.

The ultrasonic transducer acts as a band-pass device with a center frequency,  $f_0$ , and bandwidth,  $\Delta f$ . It can be modeled as a linear time-invariant (LTI) system. Its output can be described as a convolution of an input-signal characteristic and the system-response function in the time domain. The spectrum of the output signal can then be calculated as the product of Fourier transforms of the input signal and the transducer response (32). For an ideal ultrasonic transducer, the spectrum,  $h(\omega)$ , can be expressed by the following formula:

$$h(\omega) = e^{-\left[\frac{(\omega - \omega_0)^2}{1601.1 \left(\frac{1}{Q}\right)^2}\right]} \quad [1]$$

where  $\omega_0$  is angular frequency,  $Q$  is  $f_0/\Delta f$ . The amplitude coefficient was normalized.

According to Huygen's principle, the ultrasonic field at any given point in the space above the transducer surface is the sum of contributions from all the Huygen's sources. For a broad-band transducer, the sound pressure at any given point in the ultrasound field is a composite of all frequency components of the transducer's radiating pressure. Therefore, the total sound pressure, consisting of various frequency components, is an integral of the single-frequency component over the transducer bandwidth and the transducer surface (32–34):

$$P(r, \varphi, f_0, \Delta f) = \int_{\omega_0 - \Delta\omega}^{\omega_0 + \Delta\omega} [h(\omega) \frac{j\rho\omega}{2\pi} P_0] \int_0^a \sigma d\sigma \int_0^{2\pi} \frac{e^{-j\frac{\omega}{c}\sqrt{r^2 + \sigma^2 - 2r\sigma\sin\varphi\cos\theta}}}{\sqrt{r^2 + \sigma^2 - 2r\sigma\sin\varphi\cos\theta}} d\theta d\omega \quad [2]$$

In Equation 2,  $\rho$  is the density of soft tissue,  $\omega$  is the angular frequency of the sound wave,  $P_0$  is the peak amplitude of pressure on the transducer face,  $a$  is the radius of the transducer,  $\sigma$  is the radial distance from any point,  $p$ , on the transducer surface to the center of transducer,  $\theta$  is the angle between any point,  $p$ , on the transducer surface and  $x$  axis,  $c$  is the speed of sound

propagating in soft tissue,  $r$  is the distance from observation point to center of transducer, and  $\phi$  is the angle between the transducer axis and the radial vector.

In the near field, we use a summation equation in place of Equation 2. Then,

$$P(r, \phi, f_0, \Delta f) = \sum_{n=1} B(f_n) C(r, \theta, f_n) e^{-j\delta_n(r, \theta, f_n)} \quad [3]$$

where  $B(f_n)$  is a spectral density function of the transducer and can be obtained from Equation 1 for various bandwidths,  $C(r, \theta, f_n)$  and  $\delta(r, \theta, f_n)$  are the amplitude and the phase of the pressure of the transducer at frequency  $f_n$ .

In the calculation, we assumed that the peak amplitude,  $P_0$ , of sound pressure at the transducer face is 1, the density of soft tissue is 1, sound velocity,  $c$ , is 1,500 m/sec, maximum value of  $n$  is 30, and the frequency interval is 0.5 MHz. Simulation results for the ultrasound field of a transducer with three different frequency bandwidths ( $\Delta f/f_0=0$  percent,  $\Delta f/f_0=30$  percent,  $\Delta f/f_0=90$  percent;  $a=1.5$  mm;  $f_0=7.5$  MHz) are shown in Figure 4. Due to the symmetry of the transducer, only the pressure characteristic in the positive XZ plane of the transducer is shown.

Several sound-field characteristics of the ultrasonic transducer are evident in Figure 10. First, the sound-pressure fluctuation in the near field is smoothed due to the presence of various harmonic components. The broader the bandwidth, the better the near-field homogeneity, indicating that a broad-band transducer is suitable for detecting shallow soft tissue layers in the near field. Second, the peak sound pressure increases more than 50 percent when the bandwidth increases from 30 percent to 90 percent. Thus, the total emitting energy increases with the increase of the bandwidth. Third, the above analysis is based on an ideal ultrasonic transducer with a Gaussian response spectrum with an electrical excitation impulse. The spectrum characteristic of an impulse function,  $\delta(t)$ , is assumed to be 1 over the frequency dimension. In the CASS, the excitation source is a square impulse with a 50 ns pulse length and 10 kHz pulse-repetition frequency. The envelope of Fourier series coefficients is a sinc function. Although the frequency bandwidth will be affected by the properties of the emitting power transducer, the bandwidth of the exciting signal can still reach 200 MHz. Therefore, the ideal transducer represents a good approximation of the actual transducer and the preceding sound-field analysis is suitable for our design.

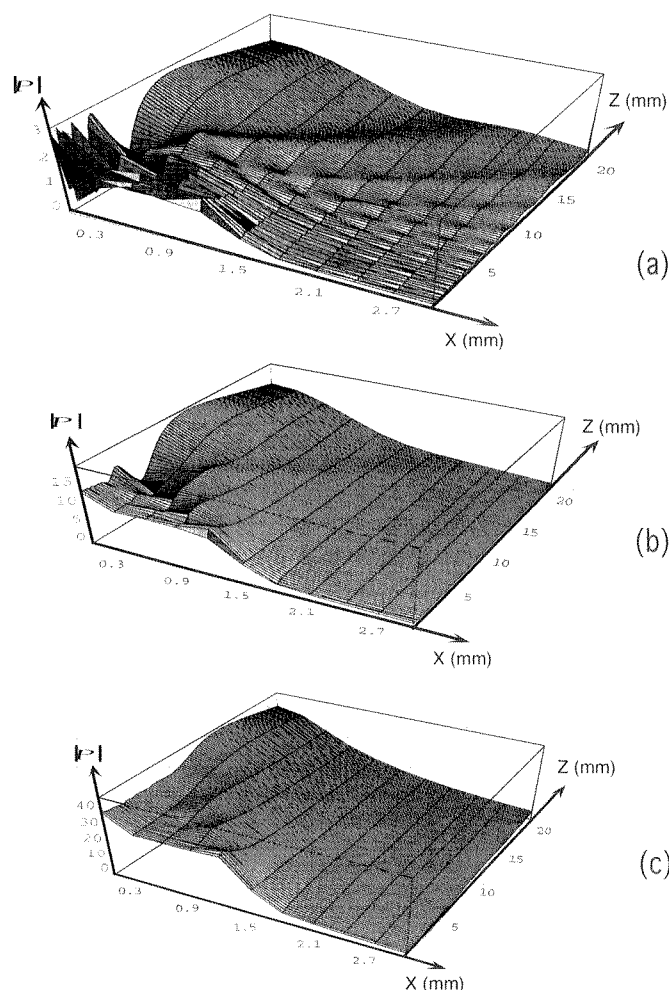


**Figure 10.**

The simulation of the near-field characteristics of an ultrasonic transducer for (a)  $\Delta f/f_0=0$  percent; (b)  $\Delta f/f_0=30$  percent; (c)  $\Delta f/f_0=90$  percent (radius=1.5 mm,  $f_0=7.5$  MHz).

## ACKNOWLEDGMENTS

The authors would like to thank Dr. C. T. Lin and Mr. Mark McCartney for their help in developing the compound sensors.

## REFERENCES

1. Hausman LL. Cost containment through reducing pressure ulcers. *Nurs Manage* 1994;25(7):88R,88T,88V.
2. Lee BY, Dasilva MC. Setting the objectives: societal values. In Lee BY and Herz BL, editors. Chapter 1 in *Surgical management of cutaneous ulcers and pressure sores*. New York: Chapman & Hall; 1998. p. 1-3.

3. AHCPR. Pressure ulcers in adults: prediction and prevention. The Agency for Health Care Policy and Research (AHCPR) Publication No. 92-0047, 1992 (May).
4. Marwick C. Recommendations seek to prevent pressure sores. *JAMA* 1992;268(6):700-1.
5. Salzberg CA, Byrne DW, Cayten CG, van Niewerburgh P, Murphy JG, Viehbeck M. A new pressure ulcer risk assessment scale for individuals with spinal cord injury. *Am J Phys Med Rehabil* 1996;75(2):96-104.
6. Allman RM, Laprade CA, Noel LB, Walker JM, Moorer CA, Dear MR, et al. Pressure sores among hospitalized patients. *Ann Intern Med* 1986;105:337-42.
7. Norton D, McLaren R, Exton-Smith AN. An investigation of geriatric nursing problems in hospital. Edinburgh: Churchill Livingstone; 1975. p. 193-238.
8. Michocki RJ, Lamy PP. The problem of pressure sores in a nursing home population: statistical analysis. *J Am Geriatr Soc* 1976;24:323-26.
9. Nola GT, Vistnes LM. Differential response of skin and muscle in the experimental production of pressure sores. *Plast Reconstr Surg* 1980;66(5):728-33.
10. Kosiak M. Etiology of decubitus ulcers. *Arch Phys Med Rehab* 1961(Jan);42:19-29.
11. Crenshaw RP, Vistnes LM. A decade of pressure sore research: 1977-1987. *J Rehabil Res Dev* 1989;26(1):63-74.
12. Levine SP, Kett RL, Ferguson-Pell M. Tissue shape and deformation versus pressure as a characterization of the seating interface. *Assist Technol* 1990;2(3):93-9.
13. Todd BA, Thacker JG. Three-dimensional computer model of the human buttocks, *in vivo*. *J Rehabil Res Dev* 1994;31(2):111-9.
14. Bennett L, Kavner D, Lee BY, Trainor FS, Lewis JM. Skin stress and blood flow in sitting paraplegic patients. *Arch Phys Med Rehabil* 1984;65(4):186-90.
15. Reddy NP, Palmieri V, Cochran GB. Evaluation of transducer performance for buttock-cushion interface pressure measurements. *J Rehabil Res Dev* 1984;21(1):43-50.
16. Graebe RH. Cushioning to benefit tissue viability. 1984.
17. Reddy NP, Palmieri V, Cochran GV. Subcutaneous interstitial fluid pressure during external loading. *Am J Physiol* 1981; 240(5):327-9.
18. Reger SI, et al. Deformation and stiffness of soft tissues by magnetic resonance imaging. In The 8th Annual IEEE/Engineering in Medicine and Biology Society Conference. 1986. New York.
19. Brienza DM, Chung KC, Brubaker CE, Wang J, Karg TE, Lin CT. A system for the analysis of seat support surfaces using surface shape control and simultaneous measurement of applied pressure. *IEEE Trans Rehabil Eng* 1996;4(2):103-13.
20. Brienza DM, Karg PE, Brubaker CE. Seat cushion design for elderly wheelchair users based on minimization of soft tissue deformation using stiffness and pressure measurements. *IEEE Trans Rehabil Eng* 1996;4(4):320-8.
21. Wang J, Brienza DM, Brubaker CE, Yuan YW. Design of an ultrasound soft tissue characterization system for the computer-aided seating system. Proceedings of 19th Annual RESNA Conference, Salt Lake City, Utah, June 7-12, 1996.
22. Sehgal CM, Lewallen DG, Nicholson JA, Robb RA, Greenleaf JF. Ultrasound transmission and reflection computerized tomography for imaging bones and adjoining soft tissues. Proceedings of the IEEE 1988 Ultrasonics Symposium 2. 1989. p. 849-52.
23. Krouskop TA, Dougherty DR, Vinson FS. A pulsed Doppler ultrasonic system for making non-invasive measurements of the mechanical properties of soft tissue. *J Rehabil Res Dev* 1987;24(2):1-8.
24. Kadaba MP, et al. Feasibility of using ultrasound to detect incipient pressure sores. *Annals of Biomed Engineer, J Biomed Eng Soc* 1991.
25. Clark M, Rowland LB, Wood HA, Crow RA. Measurement of soft tissue thickness over the sacrum of elderly hospital patients using B-mode ultrasound. *J Biomed Eng* 1989;11(3):200-2.
26. Ophir J, Cespedes I, Ponnekanti H, Yazdi Y, Li X. Elastography: a quantitative method for imaging the elasticity of biological tissues. *Ultrasound Imaging* 1991;13(2):111-34.
27. Zheng YP, Mak AFT. An ultrasound indentation system for biomechanical properties assessment of soft tissues *in vivo*. *IEEE Trans Biomed* 1996;43(9):912-7.
28. Brienza DM, Chung KC, Brubaker CE, Kwaitkowski RJ. Design of a computer-controlled seating surface for research application. *IEEE Trans Rehabil Eng* 1993;1(1):63-6.
29. Kwaitkowski RJ, Inigo RM. A closed loop automated seating system. *J Rehabil Res Dev* 1993;30(4):393-404.
30. Smith WA, Auld BA. Modeling 1-3 composite piezoelectrics thickness-mode oscillations. *IEEE Trans Ultrason, Ferroelect, Freq Contr* 1991;38(1):40-7.
31. Certon D. Theoretical and experimental investigations of lateral modes in 1-3 piezocomposites. *IEEE Trans Ultrason, Ferroelect, Freq Contr* 1997;44(3):643-51.
32. Oppenheim AV, Willsky AS, with Nawab SH. Signals and systems. Upper Saddle River, NJ: Prentice-Hall; 1997. p. 69-94.
33. Zemanek J. Beam behavior within the nearfield of a vibrating piston. *J Acoust Soc Am* 1971;49(1):181-91.
34. Papadakis EP, Fowler KA. Broad-band transducers: radiation field and selected applications. *J Acoust Soc Am* 1971;50(3):729-45.

Submitted September 2, 1999; accepted December 14, 1999.